A Validation Study of Full-Scale CFD Simulation for Sea Trial Performance Prediction of Ships

X International Conference on Computational Methods in Marine Engineering
MARINE 2023
J. García-Espinosa, L. González, J.E. Gutiérrez & B. Serván-Camas (Eds)

A Validation Study of Full-Scale CFD Simulation for Sea Trial Performance Prediction of Ships

Kadir Burak Korkmaz[1*], Keunjae Kim[1], Mattias Liefvendahl[1], Sofia Werner[1] and Michal Orych[†]

[1] RISE-SSPA Sweden AB, 400 22 Gothenburg, Sweden, web page: http://www.ri.se

[†] FLOWTECH International AB, 400 22 Gothenburg, Sweden, web page: http://www.flowtech.se

[*] Corresponding author: Kadir Burak Korkmaz, burak.korkmaz@ri.se

ABSTRACT

Shipping is a critical component of global trade but also accounts for a substantial portion of global greenhouse gas emissions. Recognising this issue, the International Maritime Organisation (IMO) has implemented new measures aimed at determining the energy efficiency of all ships and promoting continuous improvements, such as the Energy Efficiency Existing Ship Index (EEXI). As Computational Fluid Dynamics (CFD) can be used to calculate the EEXI value, RISE-SSPA[1] and Flowtech have developed a CFD-based method for predicting full-scale ship performance with SHIPFLOW v7.0, which meets the new requirements of IMO. The method is validated through an extensive comparison study that examines the delivered power and propeller rotation rate between full-scale CFD predictions and high-quality sea trials using 14 common cargo ships of varying sizes and types. The comparison between the CFD predictions and 59 sea trials shows that both delivered power and RPM can be predicted with satisfactory accuracy, with an average comparison error of about 4% and 2%, respectively. The numerical methods used in this study differ significantly from the majority of the state-of-the-art CFD codes, highlighting their potential for future applications in ship performance prediction. Thorough validation with a large number of sea trials is essential to establish confidence in CFD-based ship performance prediction methods, which is crucial for the credibility of the EEXI framework and its potential to contribute to shipping decarbonisation.

Keywords: CFD; full-scale; quality assurance; ship hydrodynamics; self-propulsion

1. INTRODUCTION

Seaborne transportation mobilises the vast majority of the cargo worldwide by common cargo vessels. However, the crucial role of shipping in global trade is realised while emitting 2.89% of Global Greenhouse Gas (GHG) emissions (IMO, 2021). In addition, the future projections on long-term economic and energy scenarios of the International Maritime Organisation (IMO) indicate that shipping emissions need to be reduced according to the goals set by IMO (2021). In line with this vision, one of the possible paths to reduce shipping emissions is increasing ships' energy efficiency. Therefore, IMO has been introducing regulations to mitigate the GHG emissions from ships. An earlier example is the introduction of the Energy Efficiency Design Index (EEDI) (IMO, 2011), which aims to eliminate

[1]SSPA Sweden AB has become a fully integrated part of the RISE Research Institutes of Sweden since 01-01-2023.

inefficient ships to join the global fleet and to promote higher energy efficiency ship designs. EEDI calculations are now a mandatory step where the applicable ships are pre-verified with towing tank tests during the design phase of a new ship.

IMO introduced a new regulation mandating the calculation of the Energy Efficiency Existing Ship Index (EEXI) for all ships (IMO, 2022). Similar to the previously introduced EEDI, the EEXI calculations aim to obtain energy efficiency indications for existing ships. The new regulation requires that all vessels, including those built before the introduction of the EEDI regulation, undergo the calculation of the Energy Efficiency Existing Ship Index. As stipulated by (IMO, 2022), the calculated EEXI value for each individual ship must be below the required EEXI. Thus, a minimum energy efficiency standard is established for all ships. If towing tank tests are available for the vessel, the EEXI value can be calculated from the extrapolated speed-power relations. However, towing tank tests may not be available for all existing ships. Therefore, IMO (2022) has agreed to accept Computational Fluid Dynamics (CFD) results for calculating the EEXI value.

The requirements for the numerical methods and their usage to produce a speed-power curve for EEXI calculations are described in IACS (2022). According to the IACS guidelines, not only the model scale computations but also the full-scale CFD can be performed. The model scale CFD methodology has been verified and validated for decades and reached an acceptable maturity level in terms of resistance, self-propulsion, and local flow predictions (Hino et al., 2020). However, the verification and validation effort for the full-scale CFD computations is relatively new and lagging behind mainly due to a lack of publicly available full-scale data, i.e. sea trials. Lloyd's Register conducted a full-scale numerical modelling workshop with a blind test case for validation. The results of the workshop, as summarised by Ponkratov (2016), offer valuable insights into the performance of various numerical modelling techniques. Upon closer analysis of the published results, it was found that the mean comparison error for the predicted power was 13% for all submissions, indicating a certain degree of variability in the accuracy of the models. Nevertheless, it is worth noting that three out of the twenty-seven participants achieved highly accurate results, with errors below 3% for all considered speeds. In addition, recent publications such as Orych et al. (2021); Sun et al. (2020); Mikulec and Piehl (2023); Mikkelsen and Steffensen (2016); Niklas and Pruszko (2019); Schouten et al. (2022) demonstrated good accuracy of predicting sea trial conditions with full-scale CFD. However, most of the full-scale validation studies in the literature are performed on a ship with one or a limited number of sea trials. As discussed in Korkmaz et al. (2021), a large number of sea trials are required for full-scale validations since the uncertainty of each trial is large.

The three steps listed in the IACS guidelines for the applicability of the CFD method are the demonstration of qualification, validation/calibration and calculation. This study focuses on the demonstration of qualification (Step 1) following the procedure recommended by ITTC (2021b). Therefore, the computational methods and the development of the Best Practice Guidelines (BPG) are discussed in Section 2. In addition, the results of an extensive comparison study performed with fourteen vessels and 59 sea trials between the full-scale CFD predictions and sea trials are discussed in Section 4.

The numerical techniques employed in the current study for full-scale computations considerably differ from many state-of-the-art CFD codes. Specifically, the study employs structured and overlapping grids, no-slip wall treatment, free-surface treatment, and propeller modelling. As a result, the current research could offer crucial insights and experiences into these techniques. Additionally, the study highlights the importance of meticulous validation work in establishing quality assurance and confidence, which is imperative for ensuring the credibility of the Energy Efficiency Existing Ship Index (EEXI) framework and its potential to facilitate the decolonisation of the shipping industry.

2. COMPUTATIONAL METHODS

This study utilises the SHIPFLOW version 7.0 CFD solver for its simulations, employing the potential flow solver XPAN to compute heave and pitch Janson (1997) and the steady-state RANS solver XCHAP for full-scale self-propulsion simulations (Broberg et al., 2022).

Featuring higher-order panels and singularity distributions, XPAN is a nonlinear Rankine source panel method (Janson, 1997). The iterative process for the nonlinear free surface boundary condition, which applies nonlinear boundary conditions to the free surface, calculates dynamic sinkage and trim. During each iteration, the ship's position is adjusted, and the panelization of the hull and free surface is updated. The heave and pitch obtained are then used to position the hull in the RANS simulations through one-way coupling.

The steady, incompressible Reynolds Averaged Navier-Stokes (RANS) equations are solved by XCHAP using a finite volume method. The Explicit Algebraic Stress Turbulence Model (EASM) is implemented in this paper Deng et al. (2005). Wall functions are not used, and the equations are integrated up to the wall. The Roe scheme discretises the convection (Roe, 1981), while a central scheme is employed for the diffusive fluxes. Explicit flux correction is applied to achieve second-order accuracy (Dick and Linden, 1992), (Chakravarthy and Osher, 1985). The Volume of Fluid Method (VOF) is used to handle the water-air interface.

By modifying the boundary conditions for the specific dissipation of turbulent kinetic energy, ω, and turbulent kinetic energy, k (Orych et al., 2022a), the hull roughness effect is modelled. The equivalent sand grain roughness height, k_S, is employed for quantifying roughness.

Structured grids are utilised in XCHAP. For a bare hull case, a single block grid is typically generated, while multi-block structured or overlapping grids are used for more complex geometries, such as hulls with appendages and local grid refinements.

To account for the propeller's effect, body forces are introduced. As the flow traverses the propeller swept volume, its linear and angular momentum increase as if interacting with a propeller with an infinite number of blades. The forces, spatially varying but time-independent, produce a propeller-induced steady flow. A built-in lifting line propeller analysis program calculates the body forces (Zhang, 1990). Furthermore, a friction resistance component is considered, which contributes to the propeller torque. This simplified modelling approach also addresses blade roughness.

An iterative procedure is used for body force computation. Initially, the current velocity field approximation is extracted at a representative propeller plane. The induced propeller wake is subtracted to obtain the effective wake, which is determined by the circulation from the previous iteration in the lifting line method. New circulation and forces are computed within the effective wake. These forces are then distributed across the volume cells in the cylindrical grid. The body forces are incorporated into the flow equations' right-hand side, resulting in a new velocity field after solving the equations. Body forces are updated with each iteration. Upon convergence, the total wake calculated by the RANS solver and the lifting line method should correspond in the chosen propeller plane.

For self-propulsion simulation, the program automatically adjusts the propeller rotational speed to achieve equilibrium between resistance and thrust (ITTC, 2017).

The development of the best practice guidelines with SHIPFLOW for full-scale self-propulsion free-surface RANS computations has been initiated from the model-scale investigations that span over decades (Liefvendahl, 2023). The computation of the resistance with the double-body RANS approach

has been extensively verified, and validated, and best practice guidelines have been developed in Korkmaz et al. (2021). The self-propulsion capabilities of the SHIPFLOW code have been successfully demonstrated by Kim and Li (2010) and Korkmaz et al. (2015). Additionally, verification, validation, and in-depth investigations have been performed on the lifting line model for open water and in behind conditions (Korkmaz, 2015). The free-surface RANS capabilities of SHIPFLOW in model scale have been demonstrated by an extensive validation study where a wide range of transom shapes and Froude numbers have been covered in Orych and Larsson (2015). A Verification and Validation (V&V) study has been carried out for self-propulsion simulations using free-surface RANS (Orych and Regnström, 2023). The surface roughness modelling for full-scale computations has been investigated, and the implementation of different models is discussed in Orych et al. (2022b). In Orych et al. (2021), a V&V study has been performed in full scale. It was demonstrated that the full-scale delivered power comparison error between the CFD prediction and sea trials is significantly smaller than the validation uncertainty, indicating numerical and modelling errors are well within acceptable levels in full scale. Based on both published and internal studies, a best practice guideline for full-scale self-propulsion free-surface RANS computations. The SHIPFLOW best-practice guidelines fulfil the requirements of IACS guidelines (IACS, 2022).

3. TEST CASES AND COMPUTATIONAL CONDITIONS

The test cases comprise fourteen common cargo vessels which were towing tank tested at RISE-SSPA earlier. As the speed trials of some vessels were performed at more than one loading condition, the total number of test cases is nineteen. The L_{PP} of the vessels range from approximately 175 m to 350 m, block coefficients (C_B) vary between 0.52 and 0.84, and the Froude numbers (the achieved speed at 75% MCR) are covering the range of 0.14 to 0.23.

Eleven of the fourteen vessels were built in series, and speed trials were performed for each sister ship. For three vessels, one speed trial is available per vessel. The data set consists of 59 sea trials in total. The trial measurements were conducted by the yards and analysed by RISE-SSPA with in-house software according to ITTC Recommended Procedures and Guidelines for Preparation, Conduct and Analysis of Speed/Power Trials (ITTC, 2017b) and ISO Ships and marine technology—Guidelines for the assessment of speed and power performance by analysis of speed trial data (ISO, 2015). The trials fulfil the ISO 15016/ITTC limits on weather conditions. The corresponding model tests were conducted at RISE-SSPA.

The hull, propeller and appendage geometries used in the full-scale computations were identical to the earlier towing tank tests. Similarly, the computational conditions replicate the same conditions as the full-scale predictions from the towing tank tests, such as calm and deep waters with seawater properties corresponding to 15°C. The geometry of the superstructure is not included in the computations; therefore, the air resistance is included as an external force in the computations. The air resistance is calculated from the air resistance coefficient as described in ITTC (2021d) using the transversal projected area of the ship above the waterline.

As most hulls have more than one speed trial and the speed attained at each trial differs between the sister ships, it is not practical to simulate the sea trial speeds directly. Instead, at least three ship speeds were computed for each test case. The speeds used for the full-scale computations are adopted from the Froude numbers tested earlier in the towing tank tests.

4. RESULTS

This section presents an extensive validation study between the sea trial measurements and CFD predictions, as required in the demonstration of the quality step of the ITTC Quality Assurance (QA) Procedure (ITTC, 2021c). Each CFD computation has been performed according to the best practice guideline developed for full-scale self-propulsion free-surface RANS computations. It means that in addition to the computational setup, the grid resolution of each hull is highly similar, thanks to the parametric nature of the structured grid generation in SHIPFLOW. An example of the grid distribution on the no-slip surfaces (i.e. hull and the appendages), the wave elevation and the effective wake generated by the lifting line model is presented in Fig. 1.

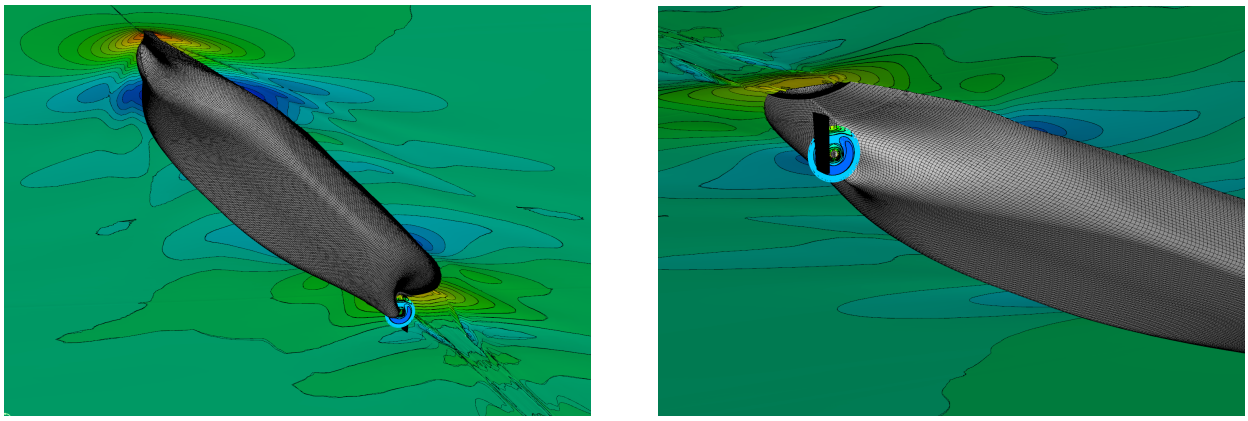

(a) Perspective view from the bow (b) Perspective view from the stern

Figure 1: Free surface wave elevation, effective wake and the grid distribution on the appended hull

4.1 Sea Trial Analysis

The combination of the precision and bias limits of single speed trial result is approximately 10% of total uncertainty as indicated by Werner and Gustafsson (2020) and Insel (2008). Therefore, comparing the CFD predictions and a limited number of speed trials will likely be inconclusive. Instead, a large number of sea trials are required for a statistically meaningful comparison between the trials and CFD predictions since the uncertainty of each trial is substantial.

As explained in Section 3, the full-scale computations were not performed at speed attained at each speed trial. Instead, as seen in Fig. 2, three speeds were computed for one of the test cases and a polynomial curve is fitted to the computed values for the delivered power (P_{DT}) and propeller turning rate (rps). The computed power and rps values are then obtained from the speed-power and speed-rps curves at the same speed as the attained speed at the sea trial.

The comparison between the speed trial measurement and the computations were quantified similarly to the correlation factors ($C_P - C_N$) (ITTC, 2017a) in the 1978 Power Prediction method (ITTC, 2021a). The correlation of each individual speed trial, $C_P^{'}$ and $C_N^{'}$, are calculated as

$$C_P^{'} = \frac{P_{D\ trial}}{P_{D\ CFD}} \quad \text{and} \quad C_N^{'} = \frac{n_{trial}}{n_{CFD}} \tag{1}$$

where the $P_{D\ trial}$ and n_{trial} are the power and propeller turning rate from a speed trial, while $P_{D\ CFD}$ and n_{CFD} represent the corresponding predictions based on the model test. Note that in IACS

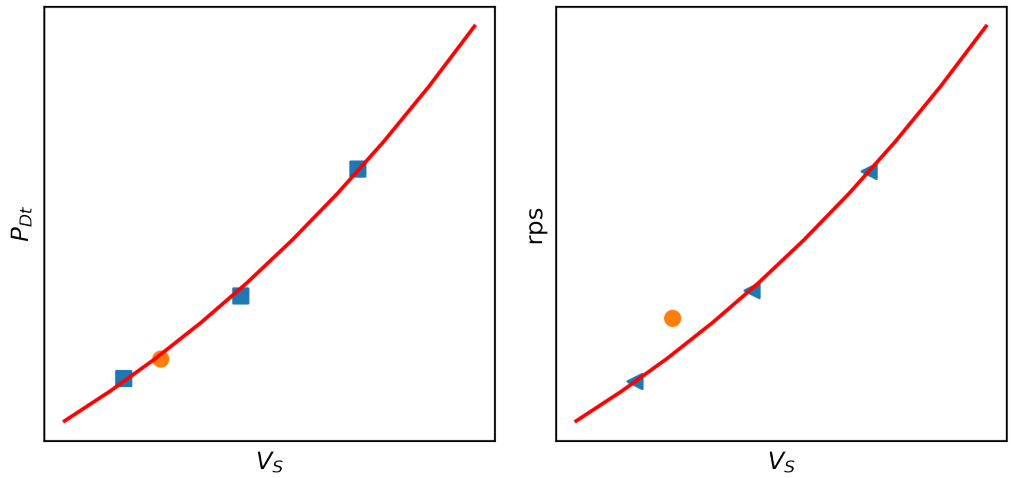

Figure 2: Power and propeller turning rate versus ship speed for computed (blue square markers) and measured (orange circle markers) values

guidelines (IACS, 2022), $C_P^{'}$ and $C_N^{'}$ are named as calibration factors which is the ratio between the sea trial power and the numerical calculation found power.

After $C_P^{'}$ and $C_N^{'}$ are calculated for each sea trial, an assembled correlation factor for C_P and C_N are determined by taking the median of $C_P^{'}$ and $C_N^{'}$ of all trials of sufficient quality (Werner and Gustafsson, 2020). The assembled correlation factors are used in towing tank testing practice as "correction for any systematic errors in model test and powering prediction procedure, including any facility bias" (ITTC, 2017a). In this study, C_P and C_N will be used to correct the CFD results, which corresponds to the current CFD setup, i.e. best practice guidelines. The Probability Density Functions (PDFs) and histograms of $C_P^{'}$ and $C_N^{'}$ are presented by shifting the median of PDFs to 1, i.e. multiplication of individual correlation factors with the assembled C_P and C_N, respectively.

4.2 Comparison between the CFD predictions and speed trials

The histograms and the probability density functions of the normalised correlation factors, $C_P(CFD)$ and $C_N(CFD)$, are calculated for each speed trial. In addition to the normalised PDF curve, the probability density function of the correlation factors before the correction is also displayed together with the standard deviation (σ) and the mean of $C_P(CFD)$ and $C_N(CFD)$ in Fig. 5. The mean of PDF are 0.96 and 1.02 for $C_P^{'}$ and $C_N^{'}$. This indicates that the mean comparison error between the CFD predictions and the sea trials is 4% and 2% for delivered power and propeller turning rate, respectively. In addition, the mean absolute comparison error (before C_P and C_N correction) is 5.6% and 3.3% for the delivered power and propeller turning rate.

After assembled C_P and C_N corrections, the histogram and the probability density function derived from the normal distribution are highly similar for both the power and propeller turning rates. Thus, the comparison error, e.g. $C_P(CFD)$-1, is also normally distributed, and no significant bias exists between the predictions and trial measurements.

Comparing the standard deviations for the power and RPM predictions indicates that the scatter is significantly lower for the propeller turning rate. In other words, the propeller turning rate prediction is more accurate ($\sigma = 0.036$) than the delivered power prediction ($\sigma = 0.060$). Assuming normal

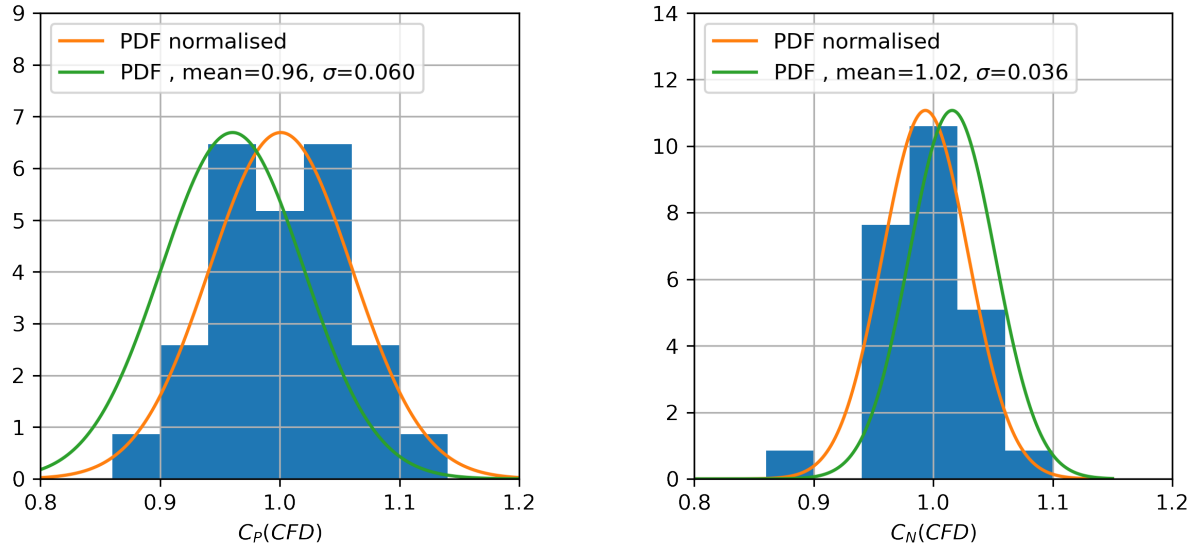

(a) Delivered power

(b) Propeller turning rate

Figure 3: Histogram and probability density functions of the $C_P(CFD)$ and $C_N(CFD)$

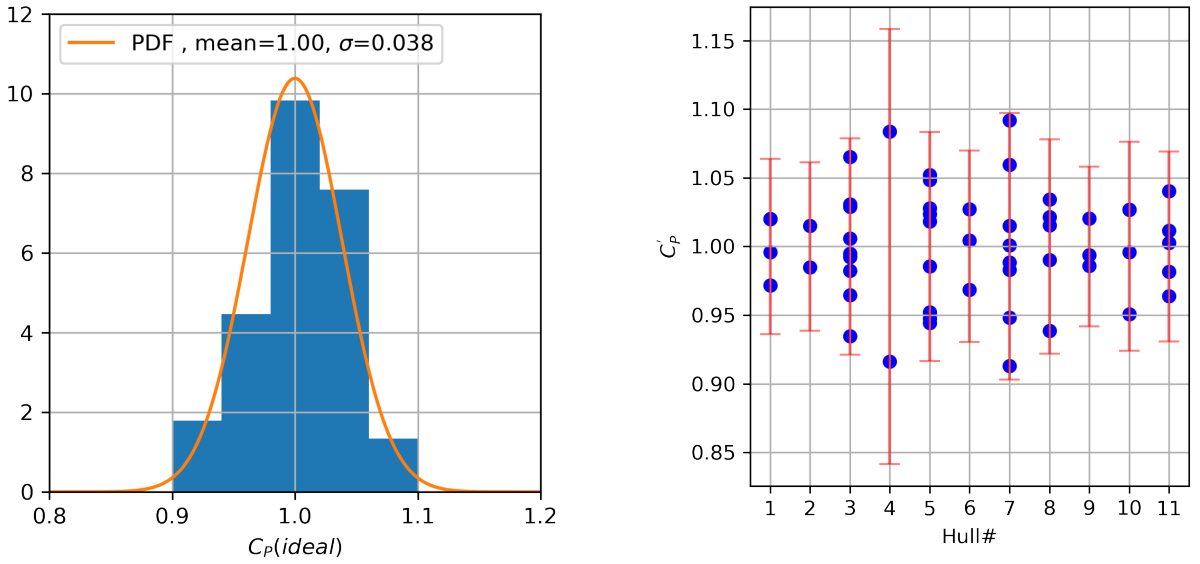

(a) Delivered power

(b) Scatter among the sister vessels for the delivered power

Figure 4: Histogram and probability density function of the delivered from the ideal case and individual trials for each hull

distribution is valid, the standard deviations indicate that 95% of the speed trials were predicted by CFD within ±12% and ±7% accuracy for power and RPM, respectively.

At first glance, the accuracy of the CFD predictions may not look too impressive; however, a considerable part of the standard deviation is caused by the scatter in the speed trials of the sister ships as argued by Korkmaz et al. (2021). To illustrate this, an ideal prediction scenario has been prepared using cases with more than one speed trial. The ideal case means the CFD prediction is identical to

the speed trial measurement. However, since the speed trial measurements between the sister ships vary, the ideal case would be that the mean C_P' of a series of sisters would be 1. The resulting C_P' values for the vessels with more than one speed trial are presented in Fig. 4b as blue markers. In order to indicate the uncertainty of the speed trials for each vessel, the standard deviation of the C_P' values for a given hull is combined with the bias limit (U_{bias}) of 4% as estimated by Insel (2008). The resulting total uncertainty estimations ($\sqrt{\sigma^2 + U_{bias}^2}$) are indicated in Fig. 4b as error bars for each hull. As seen in Fig. 4b, the scatter among the sister ships varies significantly vessel by vessel, and the measured power at the trial can vary up to 18% between the sister ships.

Similar to the earlier plots, the histogram and the probability density function of the ideal prediction case (including hulls with one speed trial) are presented in Fig. 4a. The comparison between the predictions and the ideal case shows that more than half of the scatter indeed originates from the scatter among the sister ships. The standard deviation from the ideal prediction case is 0.038, meaning that 95% of the speed trials can be predicted within ±7.6% accuracy in the best-case scenario, while the CFD predictions were within ±12% accuracy. This comparison indicates that the accuracy of the CFD is within acceptable levels considering the bulk of the scatter originates from the differences between the sister ships.

4.3 Prediction of the delivered power and propeller turning rate

The prediction accuracy of the delivered power and propeller turning rate have been discussed individually through statistical analysis. However, a successful full-scale performance prediction requires both power and RPM to be predicted with reasonable accuracy simultaneously. To visualise if this is the case with the full-scale CFD predictions, the normalised correlation factors for the power and the propeller turning rate are plotted against each other in Fig. 5. The predictions are differentiated with varying colour and marker types in the respective loading conditions. In addition, a light blue uncertainty band extending between ±8% for $C_P(CFD)$ and ±4% for $C_N(CFD)$ is plotted. As observed in Fig. 5, the majority of the predictions are within the marked uncertainty band, indicating that the delivered power and propeller rotation rate are predicted with an acceptable accuracy at the same time.

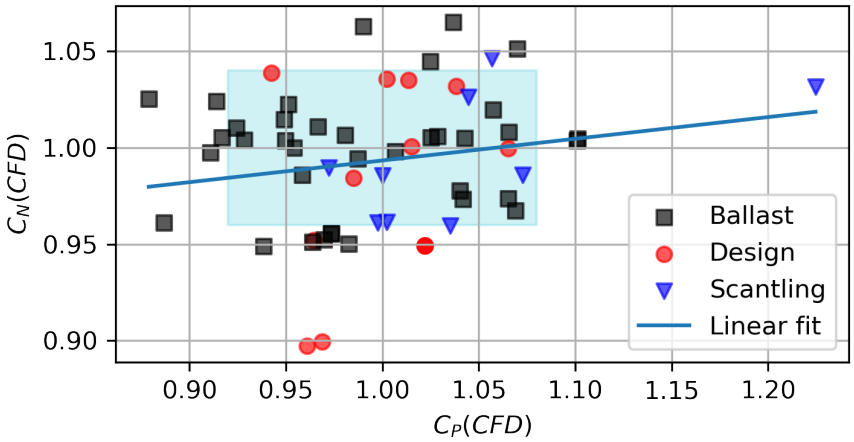

Figure 5: Correlation factors $C_P(CFD)$ versus $C_N(CFD)$

The predictions for different loading conditions are somewhat randomly distributed within the uncertainty band. There are two outliers (more than two standard deviations from 1) for $C_N(CFD)$ belonging to the Hull number 5 (see Fig. 4b), which has 6% variation between trials. The other outlier is in the delivered power prediction of the Hull number 4 (see Fig. 4b), which shows a variation of 18% difference between the trials. It can be concluded that the large scatter between the sister ships may be partially the reason for the outliers. Excluding the exceptions, no distinctive bias can be observed for predicting a particular loading condition. More definitive conclusions regarding bias for the predictions at different loading conditions can be achieved with more speed trial samples at design and scantling loading conditions.

5. CONCLUSIONS

This study presents a CFD-based method for predicting full-scale ship performance, which meets the new requirements of IMO. An extensive comparison study was performed with fourteen vessels and 59 sea trials between the full-scale CFD predictions and sea trials, where the CFD setup and grid generation were consistently according to the best practice guidelines for all test cases.

The comparison between the CFD predictions and the sea trial showed that the mean comparison error is 4% and 2% for delivered power and propeller turning rate, respectively. The histograms of the ratio between a sea trial and corresponding CFD prediction for the delivered power and propeller turning rate, i.e. correlation factor, are distributed similarly to a normal distribution. Therefore, the comparison error after the corrections on delivered power and propeller turning rate can also be assumed normally distributed, and no significant bias can be observed between the predictions and trial measurements.

The relatively large standard deviation of the correlation factors for the delivered power should be considered with care. As illustrated by an ideal prediction scenario, more than half of the standard deviation originates from the scatter among the sea trials of sister ships; hence, highlighting the significance of an extensive validation study.

A successful full-scale performance prediction method requires both power and RPM to be predicted with reasonable accuracy simultaneously, as it is critical for the engine selection. As observed from the analysis of individual correlation factors, the CFD-based method employed in this study can predict the delivered power and propeller rotation rate with acceptable accuracy at the same time. In addition, no distinctive bias was observed in predicting a particular loading condition.

The CFD method used in the current research relies on numerical techniques that differ significantly from many state-of-the-art CFD codes. These techniques provide valuable insights and experiences for future research in this field. Additionally, the study emphasises the importance of meticulous validation work to ensure the quality assurance and confidence needed to establish the credibility of the Energy Efficiency Existing Ship Index (EEXI) framework. Further studies with more test cases are needed, especially where the sea trials are available at design and scantling loading conditions to further enhance the confidence in the CFD method.

ACKNOWLEDGEMENTS

The study was mainly supported by internal strategic funding, which supports development in core competence areas. In addition, this work received funds from the Swedish Transport Agency, project LOVA TRV 2020/92054 and the Swedish Energy Agency, project ITRIM grant 2020/018759.

References

Broberg, L., Regnström, B., and Östberg, M. (2022). *XCHAP – Theoretical Manual*. FLOWTECH International AB, Gothenburg, Sweden.

Chakravarthy, S. and Osher, S. (1985). A new class of high accuracy TVD schemes for hyperbolic conservation laws. *23rd Aerospace Sciences Meeting, Reno, NV, U.S.A., AIAA paper No*, 85-0363.

Deng, G. B., Queutey, P., and Visonneau, M. (2005). Three-dimensional flow computation with Reynolds Stress and Algebraic Stress Models. In *Procedings of the ERCOFTAC International Symposium on Engineering Turbulence Modelling and Measurements; ETMM6, Sardinia, Italy, 23–25 May, 2005*, pages 389–398.

Dick, E. and Linden, J. (1992). A multigrid method for steady incompressible navier-stokes equations based on flux difference splitting. *International Journal for Numerical Methods in Fluids*, 14:1311–1323.

Hino, T., Stern, F., Larsson, L., Visonneau, M., Hirata, N., and Kim, J. (2020). *Numerical Ship Hydrodynamics: An Assessment of the Tokyo 2015 Workshop*. Springer International Publishing.

IACS (2022). Guidelines on numerical calculations for the purpose of deriving the V_{ref} in the framework of the EEXI regulation. *IACS Rec. No. 173*.

IMO (2011). *Annex 19: Resolution MEPC.203(62)*.

IMO (2021). *Fourth IMO GHG Study 2020*. International Maritime Organisation, 4 Albert Embankment, London SE1 7SR.

IMO (2022). 2022 guidelines on the method of calculation of the attained energy efficiency existing ship index (EEXI). *Annex 12: Resolution MEPC.350(78)*.

Insel, M. (2008). Uncertainty in the analysis of speed and powering trials. *Ocean Engineering*, 35(11):1183 – 1193.

ISO (2015). Ships and marine technology – guidelines for the assessment of speed and power performance by analysis of speed trial data. *15016:2015*.

ITTC (2017). *1978 ITTC Performance Prediction Method, ITTC Quality System Manual, Recommended Procedures and Guidelines*. Propulsion Committee of the 28th ITTC.

ITTC (2017a). Guidelines on the determination of model-ship correlation factors. *ITTC – Recommended Procedures and Guidelines*, 7.5-04-05-01.

ITTC (2017b). Preparation, conduct and analysis of speed/power trials. *ITTC – Recommended Procedures and Guidelines*, 7.5-04-01-01.

ITTC (2021a). 1978 ittc performance prediction method. *ITTC – Recommended Procedures and Guidelines*, 7.5-02-03-01.4.

ITTC (2021b). Quality assurance in ship CFD application. *ITTC – Recommended Procedures and Guidelines*, 7.5-03-01-02.

ITTC (2021c). Quality assurance in ship cfd application. *ITTC – Recommended Procedures and Guidelines*, 7.5–03-01–02.

ITTC (2021d). Resistance test. *ITTC – Recommended Procedures and Guidelines*, 7.5-02-02-01.

Janson, C.-E. (1997). *Potential Flow Panel Methods for the Calculation of Free-surface Flows with Lift*. Doctoral dissertation, Department of Naval Architecture and Ocean Engineering, Division of Hydromechanics, Chalmers University of Technology, Gothenburg.

Kim, K. and Li, D.-Q. (2010). Estimation of numerical uncertainty of Shipflow in self-propulsion simulation of KCS. In *Gothenburg 2010 workshop – CFD in ship hydrodynamics*, Gothenburg, Sweden.

Korkmaz, K. B. (2015). CFD predictions of resistance and propulsion for the JAPAN Bulk Carrier (JBC) with and without an energy saving device. Master's thesis, Department of Shipping and Marine Technology, Chalmers University Technology, Gothenburg, Sweden.

Korkmaz, K. B., Orych, M., and Larsson, L. (2015). CFD prediction including verification and validation of resistance, propulsion and local flow for the Japan bulk carrier (JBC) with and without an energy saving device. In *Tokyo 2015 workshop – CFD in ship hydrodynamics*, Tokyo, Japan.

Korkmaz, K. B., Werner, S., and Bensow, R. (2021). Verification and validation of CFD based form factors as a combined CFD/EFD method. *Journal of Marine Science and Engineering*, 9(1).

Liefvendahl, M. (2023). Ship power prediction with cfd in full scale. Technical Report RE71221461-01-00-A, Research Institutes of Sweden.

Mikkelsen, H. and Steffensen, M. L. (2016). Full scale validation of CFD model of self-propelled ship. Master's thesis, Technical University of Denmark, Denmark.

Mikulec, M. and Piehl, H. (2023). Verification and validation of CFD simulations with full-scale ship speed/power trial data. *Brodogradnja*, 74(1):41–62.

Niklas, K. and Pruszko, H. (2019). Full-scale CFD simulations for the determination of ship resistance as a rational, alternative method to towing tank experiments. *Ocean Engineering*, 190:106435.

Orych, M. and Larsson, L. (2015). Hydrodynamic aspects of transom stern optimization. In *5th High Performance Yacht Design Conference*, pages pp.247–256, Auckland , New Zealand.

Orych, M. and Regnström, B. (2023). Verification and validation of volume-of-fluid functionality in Shipflow. *personal communication*.

Orych, M., Werner, S., and Larsson, L. (2021). Validation of full-scale delivered power CFD simulations. *Ocean Engineering*, 238:109654.

Orych, M., Werner, S., and Larsson, L. (2022a). Roughness effect modelling for wall resolved RANS – comparison of methods. *Ocean Engineering*, 266:112778.

Orych, M., Werner, S., and Larsson, L. (2022b). Roughness effect modelling for wall resolved RANS – Comparison of methods for marine hydrodynamics. *Ocean Engineering*, 266:112778.

Ponkratov, D. (2016). 2016 workshop on ship scale hydrodynamic computer simulation. In Ponkratov, D., editor, *loyd's Register workshop on ship scale hydrodynamics*.

Roe, P. L. (1981). Approximate Riemann solvers, parameter vectors, and difference schemes. *Journal of Computational Physics*, 43:357.

Schouten, D. R., Drouet, A., Birvalski, M., and Morand, L. (2022). Full Scale CFD Validation Using Ship Performance and Wave Pattern Measurements of a Mega Cruise Ship. In *Volume 7: CFD and FSI*, page V007T08A041, Hamburg, Germany. American Society of Mechanical Engineers.

Sun, W., Hu, Q., Hu, S., Su, J., Xu, J., Wei, J., and Huang, G. (2020). Numerical Analysis of Full-Scale Ship Self-Propulsion Performance with Direct Comparison to Statistical Sea Trail Results. *Journal of Marine Science and Engineering*, 8(1):24.

Werner, S. and Gustafsson, L. (2020). Uncertainty of Speed Trials. In *5th Hull Performance & Insight Conference*, Hamburg, Germany.

Zhang, D. (1990). *Numerical Computation of Ship Stern/Propeller Flow*. Doctoral dissertation, Department of Shipping and Marine Technology, Chalmers University of Technology, Gothenburg.